Metabolic insights into metabolic dysfunction-associated steatotic liver disease: the impact of gut microbiota and TCM constitutions

Ximin Liu[1], Qiuhui Liu[2], Dongxue Lu[3]*, Zhiguang Sun[4]*

[1]Preventive Treatment Department, Changzhou Traditional Chinese Medicine Hospital Affiliated to Nanjing University of Chinese Medicine, China
[2]Department of Science and Education, Wujin Traditional Chinese Medicine Hospital, China
[3]Department of Clinical Nutrition, Academy of Health and Rehabilitation, Academy of Acupuncture and Tuina, Nanjing University of Chinese Medicine, China
[4]First Clinical Medical College, Nanjing University of Chinese Medicine, China

Submitted: 3 June 2025; **Accepted:** 12 September 2025
Online publication: 8 February 2026

Arch Med Sci 2026; 22 (4): 2098–2113
DOI: https://doi.org/10.5114/aoms/210618

***Corresponding authors:**
Zhiguang Sun
First Clinical
Medical College
Nanjing University
of Chinese Medicine
China
E-mail: zhiguangsun@njucm.edu.cn

Dongxue Lu
Department of
Clinical Nutrition
Academy of Health
and Rehabilitation
Academy of Acupuncture
and Tuina
Nanjing University
of Chinese Medicine
China
E-mail: 270773@njucm.edu.cn

Abstract

Introduction: Metabolic dysfunction-associated steatotic liver disease (MASLD) is intricately linked to gut microbiota dysbiosis and has been associated with different traditional Chinese medicine (TCM) constitution types. This study explored the fecal microbiota composition in MASLD patients to investigate the associations underlying the disease.

Material and methods: In this study, 51 MASLD patients and 46 healthy controls were classified into seven TCM constitution groups based on high-throughput sequencing of fecal samples. Analyses were conducted to compare microbial communities, metabolite profiles, and metabolic pathways among these constitution groups. The relationships between specific microbiota and biochemical indicators were evaluated using linear discriminant analysis (LDA) effect size (LEfSe) and Spearman correlation analyses.

Results: MASLD patients exhibited reduced fecal microbiota diversity compared to healthy controls, with significant variations in microbial structure among TCM constitution groups. The damp-heat constitution (DHC) and phlegm-dampness constitution (PDC) groups displayed enriched populations of specific microbial species, distinct bacterial taxa, and unique metabolite profiles. Multiple significant pathways related to amino acid, fatty acid, and carbohydrate metabolism were identified through metabolic pathway enrichment analysis. Significant correlations were observed between specific microbial taxa and biochemical indicators such as triglycerides, total cholesterol, alanine aminotransferase (ALT), and aspartate aminotransferase (AST).

Conclusions: This study highlights the close association between alterations in gut microbiota, TCM constitution differences, and MASLD progression. The findings suggest that changes in microbial diversity and metabolite profiles may contribute to MASLD pathogenesis. The identification of constitution-specific microbial may provide insights into personalized intervention strategies for MASLD.

Key words: metabolic dysfunction-associated steatotic liver disease, traditional Chinese medicine constitution, gut microbiota, 16S rRNA sequencing, metabolic pathways, personalized treatment.

Introduction

Metabolic dysfunction-associated steatotic liver disease (MASLD) is the most prevalent chronic metabolic stress-related liver disease worldwide, characterized by hepatic steatosis and lipid accumulation [1], which can progress to liver cirrhosis and even hepatocellular carcinoma (HCC) [2]. The global prevalence of MASLD is approximately 25% [3, 4], with a rising trend in China, where the prevalence currently ranges from 15% to 30% [5], making it a significant public health concern. The multifactorial etiology of MASLD involves genetic, metabolic, and environmental factors, with the gut-liver axis playing a critical role in its pathogenesis. Enhancing the accuracy of early diagnosis and timely intervention are essential to prevent disease progression and reduce the secondary risk of HCC [6]. Furthermore, studies have shown that the gut microbiota and its metabolites play pivotal roles in regulating metabolic processes, immune responses, and host defenses, closely linking them to the development and progression of MASLD [7, 8]. Moreover, increasing evidence indicates that environmental exposure to bisphenol compounds (such as BPA and its derivatives) can induce hepatic fat accumulation, elevate the risk of MASLD/metabolic dysfunction-associated fatty liver disease (MAFLD), and is closely associated with gut microbiota dysbiosis [9–11].

Recent studies have shown that the gut microbiota in MASLD patients exhibits significant dysbiosis, such as an increased Firmicutes/Bacteroidota ratio and reduced levels of Bacteroidota and Ruminococcaceae [8, 12]. Fecal microbiota transplantation experiments in high-fat diet-induced MASLD mouse models further confirm the critical role of gut microbiota in the pathogenesis of MASLD [13]. Additionally, gut microbial metabolites, including short-chain fatty acids (SCFAs, such as acetate and butyrate), trimethylamine (TMA), bile acids (BA), and ethanol, directly contribute to the mechanisms underlying MASLD [14, 15]. For example, SCFAs promote fatty acid oxidation and inhibit hepatic lipid synthesis by activating adenosine monophosphate-activated protein kinase (AMPK), thereby reducing hepatic fat accumulation [16]. These findings provide new perspectives for MASLD prevention and treatment. However, current research primarily focuses on microbial differences, lacking subgroup analyses based on individual patient characteristics.

In traditional Chinese medicine (TCM) theory, the constitution is considered the foundation of an individual's health, shaped by both innate endowment and acquired environment and is characterized by relative stability and plasticity. Wang Qi's nine-type TCM constitution classification system and diagnostic criteria hold significant importance in clinical prevention and treatment. Studies have revealed that MASLD patients predominantly present with constitutions such as yang deficiency constitution (YADC) and phlegm dampness, while liver qi stagnation constitution (QSC), spleen deficiency, and internal damp-heat constitution (DHC) are also common patterns [17]. The TCM concept that "the internal must have form, the external must have manifestation" (from *Huangdi Neijing*) suggests that the constitution reflects internal physiological changes and may have potential links with gut microbiota and metabolic characteristics [18, 19]. However, this relationship has yet to be thoroughly investigated in experimental research.

This study aimed to explore the changes in the composition of the gut microbiota in MASLD patients with different TCM constitution types and their association with metabolic characteristics. By employing 16S rRNA high-throughput sequencing technology, the study sought to identify the characteristic differences in the gut microbiota of MASLD patients with different constitution types. Metabolomics data were integrated to analyze variations in metabolite types and metabolic pathways. Through this research, we aimed to clarify the microbiota differences between different constitution types and MASLD, providing a new theoretical foundation for the personalized treatment of MASLD.

Material and methods

Patient cohort

Between June 1, 2023, and March 1, 2024, this study enrolled 51 patients with MASLD and 49 age- and sex-matched healthy controls at our hospital. The study followed the ethical principles of the Declaration of Helsinki and was approved by the Clinical Research Ethics Committee of Changzhou Hospital of Traditional Chinese Medicine, affiliated with Nanjing University of Chinese Medicine (Approval Nos. 170043 and B200357). Inclusion and exclusion criteria are detailed in Supplementary Figure S1. MASLD was diagnosed based on liver biopsy or imaging methods such as abdominal ultrasound and computed tomography, following established diagnostic criteria. Healthy controls had no history or symptoms of MASLD and had not used antibiotics, probiotics, or laxatives within 1 month before participation. Individuals were excluded if they had fatty liver due to alcohol intake (more than 140 g per week for males or 70 g for females), drug abuse, hereditary diseases, other liver diseases including viral hepatitis or autoimmune liver disease, major chronic illnesses such as malignancy, diabetes, or chronic kidney disease, were pregnant, or were unable to

complete stool sample collection or required assessments.

This study optimized constitution-based groups to ensure an adequate sample size and improve statistical power. Due to small sample sizes in certain constitution groups (e.g., QSC, blood stasis constitution (BSC), YADC, yin deficiency constitution (YIDC)), these were consolidated into two groups: DHC and phlegm-dampness constitution (PDC). After adjustment, the effect size was set at 0.7, the significance level at 0.05, and the statistical power at 0.8. Based on these statistical calculations, the sample size of 51 MASLD patients was sufficient to meet the needs of this exploratory study, ensuring the statistical validity of the analyses.

Clinical characteristics and data collection

The clinical characteristics of MASLD patients and healthy controls were assessed using standardized procedures at Changzhou Traditional Chinese Medicine Hospital, affiliated with Nanjing University of Chinese Medicine. Sample collection was conducted by trained laboratory technicians who adhered strictly to standardized protocols. Fasting venous blood samples were collected from participants in the morning. After collection, laboratory staff immediately centrifuged blood samples to separate the serum, which was then stored at –80°C until further analysis. Lipid parameters, triglyceride (TG), total cholesterol (TC), high-density lipoprotein cholesterol (HDL-C), and low-density lipoprotein cholesterol (LDL-C), were measured using enzymatic methods on a fully automated biochemical analyzer (Beckman Coulter AU5800, USA). Liver function indicators, such as ALT, AST, alkaline phosphatase (ALP), and γ-glutamyl transferase (GGT), were also analyzed using the same equipment and standardized methods. Clinical nurses recorded patient demographic information, including gender, age, height, and weight, at enrollment, and body mass index (BMI) was calculated. All data collection and testing adhered strictly to the hospital's quality control procedures, ensuring the accuracy and consistency of the results.

Assessment of TCM constitution

During patient enrollment, this study applied *the Classification and Determination of Constitution of Traditional Chinese Medicine* developed by *the Chinese Association of Traditional Chinese Medicine* to assess the TCM constitution of all participants, ensuring scientific rigor and classification accuracy. The specific procedure included the following steps: First, two TCM experts conducted consultations and observations of the patients, collecting information on tongue coating, complexion, body shape, and pulse condition. Next, participants completed a standardized *Traditional Chinese Medicine Constitution Classification Questionnaire*, where the nine basic constitution characteristics (balanced constitution, qi deficiency constitution (QDC), YADC, YIDC, PDC, DHC, BSC, QSC, and inherited special constitution) are quantified using a 5-point Likert scale. Then, based on the questionnaire scores and clinical manifestations, a standardized classification algorithm was used to classify patients into a specific constitution. For example, if a constitution type scored above 40 points and all other constitution types scored below 30, the patient was classified into that constitution type. If multiple constitution types scored above 30 points, an expert panel integrated clinical manifestations to comprehensively determine the constitution type. To ensure classification consistency, a subset of patients (n = 20) was reassessed within 1 week, and the results showed a kappa value of 0.82, indicating high reliability of the classification.

Sample collection

Fecal samples were collected for gut microbiota analysis and metabolomics research. The sample collection took place in a designated collection room at Changzhou Traditional Chinese Medicine Hospital, affiliated with Nanjing University of Chinese Medicine. Each participant received detailed instructions on the collection process, and trained professionals assisted with the procedure. Participants collected fresh fecal samples in a designated area using single-use sterile sampling tubes to prevent external contamination. After collection, healthcare staff immediately placed the samples in liquid nitrogen to prevent degradation or metabolic changes in the microbiota. All samples were stored at –80°C until they were transported to Shenzhen Microbiota Technology Co. for high-throughput sequencing analysis.

DNA extraction and 16S rRNA sequencing

Total DNA from fecal samples was extracted using the EZNA Soil Kit (Omega Bio-tek, Norcross, USA). DNA purity and concentration were measured using the NanoDrop 2000, and extraction quality was assessed by 1% agarose gel electrophoresis. The extraction process was strictly controlled in a sterile environment, with all experimental steps carried out in a laminar flow hood and using sterilized consumables to ensure the integrity and contamination-free status of the DNA samples. Polymerase chain reaction (PCR) amplification targeted the V3-V4 hypervariable regions, using primers 338F (5′-ACTCCTACGGGAGGCAGCAG-3′) and 806R (5′-GGACTACHVGGGTWTCTA-

AT-3′). The 20 µl PCR reaction mixture consisted of 9 µl of sterile double-distilled water, 4 µl of 5Fast-Pfu buffer, 2 µl of 2.5 mM dNTPs, 0.8 µl of each 5 mM primer, 0.4 µl of FastPfu polymerase, and 10 ng of DNA template. The thermal cycling program included an initial denaturation at 95°C for 3 min, followed by 27 cycles of 95°C for 30 s, 55°C for 30 s, and 72°C for 45 s, with a final extension at 72°C for 10 min (PCR instrument: ABI GeneAmp 9700). PCR products were separated by 2% agarose gel electrophoresis and purified using the AxyPrep DNA Gel Extraction Kit (Axygen Biosciences, Union City, USA). Elution was performed with Tris-HCl, and the purified products were verified by 2% agarose gel electrophoresis. DNA quantification was performed using the QuantiFluor-ST system (Promega, USA). The purified amplicons were subjected to dual-end (PE) 2300 library construction following the standard protocol for the Illumina MiSeq platform (Illumina, San Diego, USA). During sequencing, each sample was ensured to have at least 50,000 valid sequence reads to ensure sufficient sequencing depth for microbiota diversity analysis.

Microbiota analysis via 16S rDNA sequencing

Sequence read processing, quality control, OTU clustering, and taxonomic assignment were performed using the QIIME pipeline (v1.9.0). Adapter sequences and low-quality reads were removed with Trimmomatic (v0.39), ensuring Q30 quality (error rate < 0.1%) and discarding reads shorter than 100 bp. Low-quality bases at the 3′ end were trimmed using PRINSEQ (v0.20.4), and paired-end reads were merged with fastq-join. Sequence quality was assessed using FastQC (v0.11.9), and chimeric sequences were removed with USEARCH 6.1.544. OTUs were clustered using UCLUST at 97% similarity and aligned to the Greengenes reference database (v13.8). Taxonomic classification at the genus level was based on 97% sequence similarity using the Greengenes (gg_13_8) database. Alpha diversity metrics, including the Shannon index, observed species, and Chao1 index, were calculated in QIIME. Principal coordinates analysis (PCoA) using weighted and unweighted UniFrac distances and PERMANOVA were also conducted in QIIME. Differential taxa analysis was performed with LEfSe (Galaxy v1.0, The Huttenhower Lab, Harvard T.H. Chan School of Public Health), using an LDA score threshold of 2.0 and a significance level of $p < 0.05$ to ensure statistical robustness and biological relevance.

Statistical analysis

Baseline characteristics were analyzed using descriptive statistics. Quantitative variables are presented as standard deviation (SD) or interquartile range (IQR), while categorical variables are expressed as percentages. Differences in clinical indicators between groups were assessed using the χ^2 test. Depending on the distribution, Student's *t*-test or the Wilcoxon rank-sum test was applied for continuous variables. Univariate logistic regression was used to estimate crude odds ratios and their corresponding 95% confidence intervals.

GC TOF-MS experiment

GC-TOF-MS analysis was conducted using an Agilent 7000D GC/MS system (Trace 1310-TSQ8000 Evo, Thermo Fisher Scientific, USA) equipped with a TG-5MS capillary column coated with 5% diphenyl and 95% dimethylpolysiloxane. A 1 µl sample was injected in split mode, with helium as the carrier gas. The front inlet purge flow rate was set at 3 ml/min, and the column flow rate at 1 ml/min. The oven temperature was initially held at 60°C for 1 min, then increased at 10°C/min to 320°C, where it was maintained for 14 min. The injector, transfer line, and ion source temperatures were maintained at 280°C, 280°C, and 250°C, respectively. Electron impact ionization was used with an ionization energy of –70 eV. Data were acquired in full scan mode (m/z 50-500) at a scan rate of 20 spectra per second, with a solvent delay beginning at 6.27 min. Each sample was analyzed in triplicate, and internal standards were added to normalize peak intensities and ensure reproducibility.

GC-MS data preprocessing

MS-DIAL software performed peak extraction, baseline filtering, baseline calibration, peak alignment, deconvolution, and peak identification. Following this, peak area integration and mass spectrometry matching were carried out. Metabolite identification was performed by comparing with the NIST 17 and Fiehn databases to ensure the accuracy of the identification results. A data matrix was then generated, and the raw spectral files underwent preprocessing. The criteria for differential metabolite selection were fold change (FC) > 1.2 or < 0.8333, with the *p*-value set to < 0.05. To enhance the statistical significance of metabolite identification, multiple testing correction was applied to the selected results using the Benjamini-Hochberg method.

Microbiota statistical analysis

The Shannon index, observed species, and Chao1 index, which are α-diversity metrics, were assessed using Student's *t*-test. β-diversity was measured using UniFrac distance, and statistical analysis was conducted using the χ^2 test or PER-

MANOVA. Statistical significance was defined as a p-value ≤ 0.05.

Metabolomics data analysis

The Wilcoxon rank-sum test and FC analysis assessed differences in fecal metabolites between the DHC and PDC groups. Differential metabolites were then aligned with metabolic pathways by comparing them to the Kyoto Encyclopedia of Genes and Genomes (KEGG) database. A pathway was considered enriched if more than three metabolites were mapped to it, and the enrichment factor was calculated accordingly.

Results

Baseline characteristics of study participants and TCM constitution classification

This study included 51 MASLD patients and 46 healthy controls. MASLD patients were classified according to TCM constitution into the following groups: DHC (n = 14), PDC (n = 28), QDC (n = 3), QSC (n = 1), BSC (n = 2), YADC (n = 1), and YIDC (n = 2). Healthy controls did not show significant skewed constitution traits. Gender, age, and key clinical characteristics of both groups are summarized in Table I. MASLD patients had significantly higher BMI than healthy controls. However, no significant BMI differences were observed among the constitution subgroups ($p > 0.05$). TG levels were elevated in the MASLD group compared to controls ($p < 0.05$), particularly in the DHC group (2.56 ±1.41 mmol/l) and PDC group (3.8 ±1.67 mmol/l). HDL-C levels also differed significantly across constitution groups ($p < 0.05$), with the PDC group showing the lowest levels (0.56 ±0.04 mmol/l) and the DHC group slightly higher (1.01 ±0.27 mmol/l).

Liver function indicators, including AST and ALT, were elevated in MASLD patients. The highest ALT was observed in the PDC group (57.42 ±60.06 U/l), while the DHC group had lower levels (28.73 ±21.09 U/l; $p > 0.05$). Glucose (GLU) levels were elevated in the PDC group (9.78 ±2.07 mmol/l), though the difference among constitution groups was not statistically significant ($p > 0.05$). The clinical data indicate distinct metabolic patterns among MASLD patients with different TCM constitutions, with DHC and PDC groups showing more pronounced changes.

Diversity changes in the fecal microbiota of MASLD patients

To assess gut microbiota diversity and richness across different TCM constitution groups, α-diversity analysis was conducted using the Shannon, Ace, Chao1, and Simpson indices (Figures 1 A–D). The results showed variability in diversity metrics among constitution groups. The DHC and PDC groups exhibited higher Chao1 and Shannon indices, indicating greater microbial diversity and richness, while the QDC group had relatively lower values. Boxplot distributions of the Ace and Chao1 indices showed higher species richness in the YIDC group; however, none of the differences reached statistical significance ($p > 0.05$), suggesting that species richness did not differ significantly among groups.

Principal component analysis (PCA) and non-metric multidimensional scaling (NMDS) based on Bray-Curtis distances were performed to explore differences in microbiota composition. PCA revealed distinct clustering patterns in the DHC

Table I. Characteristics of the study participants

Characteristics	Qsc (n = 14)	DHC (n = 28)	BSC (n = 3)	YIDC (n = 2)	PDC (n = 2)	QDC (n = v2)	YADC (n = 2)	P-value
Sex								0.269
Male	1	9	13	2	0	0	1	
Female	2	5	15	1	1	2	0	
Age	48.57 ±14.92	50.11 ±12.33	65.67 ±8.02	53 ±1.21	65 ±5.66	61 ±2.13	65 ±2.83	0.164
Weight [kg]	75.04 ±16.28	71.96 ±11.23	76.03 ±17.53	73.37 ±0.04	57.95 ±6.43	83.47 ±16.22	64 ±5.66	0.484
BMI [kg/m^2]	26.23 ±4.01	25.59 ±3.51	27.52 ±3.72	33.97 ±0	22.9 ±2.14	28.51 ±5.09	26.63 ±4.52	0.073
TC	4.89 ±1.32	4.89 ±1.31	4.55 ±0.96	4.32 ±0.04	3.55 ±0.84	4.75 ±0.09	5.18 ±0.25	0.822
TG	2.29 ±1.29	2.56 ±1.41	1.91 ±0.26	5.62 ±0.04	3.8 ±1.67	1.1 ±0.48	1.44 ±0.13	0.014
HDL-C	1.11 ±0.22	1.01 ±0.27	1.04 ±0.1	0.61 ±0.04	0.56 ±0.04	1.05 ±0.18	1.24 ±0.21	0.02
LDL-C	2.74 ±1.21	3.21 ±1.31	2.29 ±0.36	2.57 ±0.04	2.22 ±0.78	3.07 ±0.07	3.33 ±0.35	0.695
GLU	6.37 ±2.15	7.96 ±3.46	5.96 ±1.55	4.56 ±0.04	9.78 ±2.07	4.72 ±0.76	8.4 ±1.75	0.234
ALT	26.25 ±22.19	28.73 ±21.09	33.67 ±31.56	14.97 ±0.04	26.5 ±14.85	57.42 ±60.06	19 ±2.83	0.609
AST	19.36 ±6.29	20.08 ±7.71	26 ±22.52	15.97 ±0.04	26 ±7.07	25.97 ±18.34	19 ±0.23	0.721

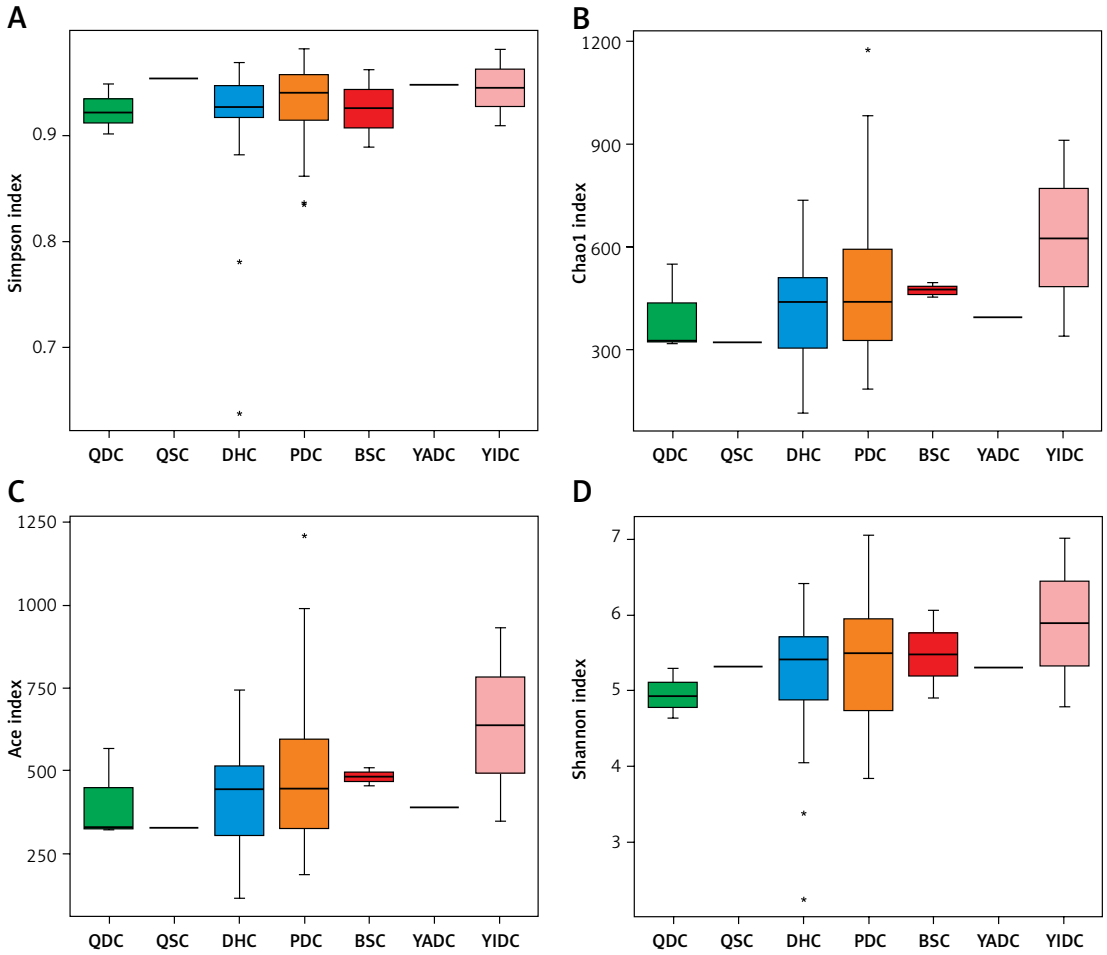

Figure 1. Gut microbiota α-diversity analysis. **A–D** – Estimation of species diversity differences across various traditional Chinese medicine (TCM) constitution groups, using the Simpson index, Chao1 index, Ace index, and Shannon index

QDC – qi deficiency constitution, QSC – qi stagnation constitution, PDC – phlegm-dampness constitution, DHC – damp-heat constitution, BSC – blood stasis constitution, YADC – yang deficiency constitution, YIDC – yin deficiency constitution.

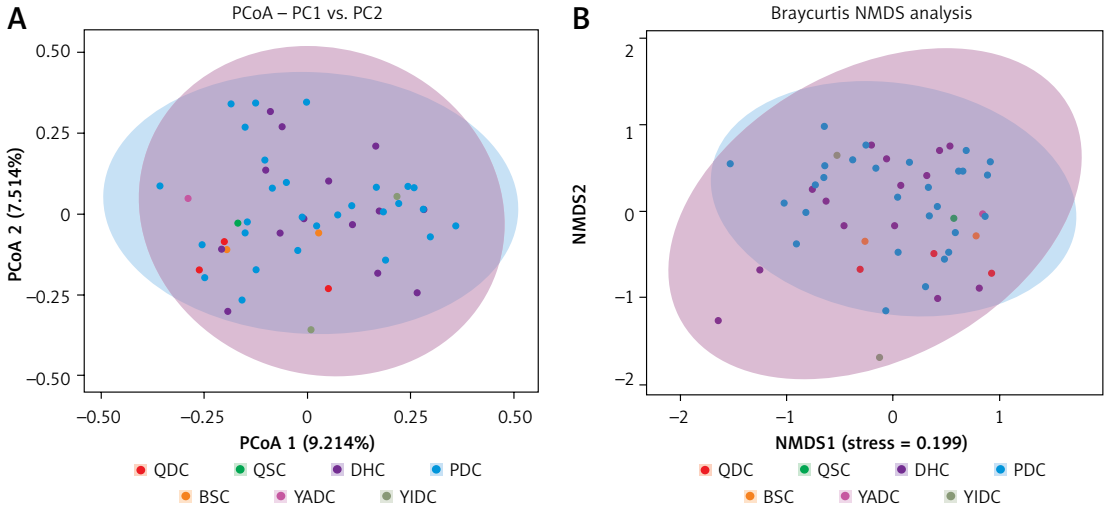

Figure 2. Gut microbiota β-diversity analysis. **A**, **B** – PCoA based on Bray-Curtis distances shows the overall microbiota composition across the seven groups. Red dots represent the QDC group, dark green dots the QSC group, blue dots the PDC group, purple dots the DHC group, orange dots the BSC group, pink dots the YADC group, and light green dots the YIDC group. Each dot represents an individual sample

and PDC groups, with these groups appearing separated from other constitution types. In contrast, groups such as QDC and QSC showed more dispersed distributions, suggesting greater variability in microbiota composition (Figure 2 A). NMDS analysis supported the observed patterns from PCA, further indicating differences in microbial community composition among the DHC and PDC groups (Figure 2 B).

Taxonomic differences in microbiota among different TCM constitution groups

Venn diagram analysis was used to assess the distribution of ASVs (amplicon sequence variants) across different constitution groups (Figure 3 A). The PDC group showed the highest number of ASVs (8620), followed by DHC (3386), YIDC (843), QDC (736), BSC (529), YADC (208), and QSC (168).

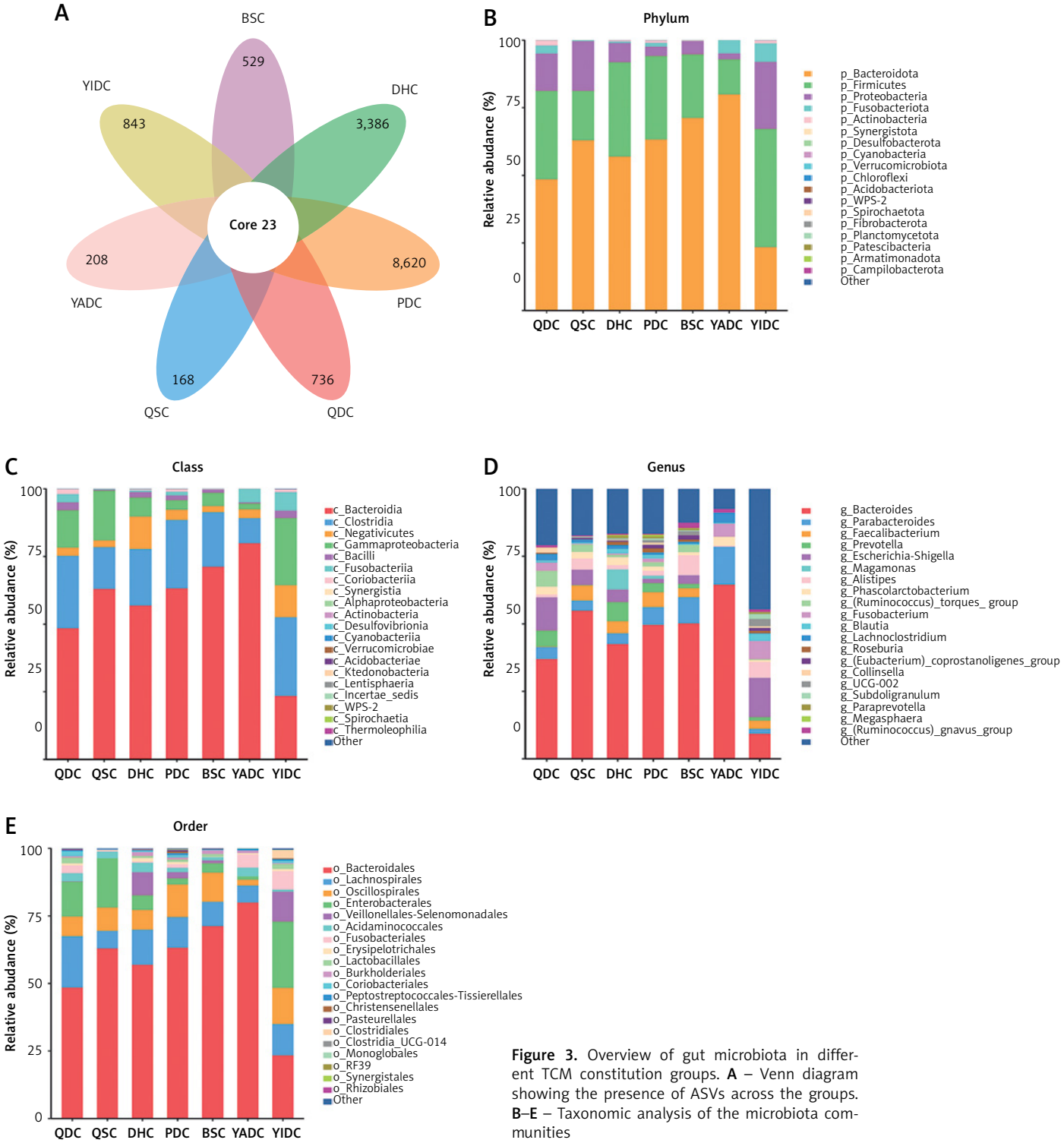

Figure 3. Overview of gut microbiota in different TCM constitution groups. **A** – Venn diagram showing the presence of ASVs across the groups. **B–E** – Taxonomic analysis of the microbiota communities

A total of 23 core ASVs were shared across all groups.

The relative abundance of microbial taxa was visualized using stacked bar charts. At the phylum level (Figure 3 B), *Bacteroidota*, *Proteobacteria*, *and Firmicutes* were dominant in all groups. *Bacteroidota* was reduced in the YIDC group, while *Proteobacteria* were notably higher in the QDC and YIDC groups. *Firmicutes* abundance was relatively increased in YIDC. At the class level (Figure 3 C), Bacteroidetes, *Clostridium*, Negativicutes, Gammaproteobacteria, and Bacilli were the major taxa. The YIDC group showed lower *Bacteroidota* and higher levels of Firmicutes and Gammaproteobacteria. At the order level (Figure 3 E), Lachnospirales abundance was elevated in the QDC and YIDC groups. *Oscillospira* was lowest in the YADC group. Enterobacterales was elevated in the QDC, QSC, and YIDC groups. At the genus level (Figure 3 D), *Bacteroides* was predominant in all groups, with higher levels in PDC and DHC. *Blautia* and *Dialister* were enriched in the QDC group. The YIDC group had the lowest *Faecalibacterium* and higher proportions of Gammaproteobacteria and Enterobacterales. *Lachnoclostridium* was more abundant in PDC and DHC, while Prevotella was enriched in DHC. *Oscillospira* showed the lowest abundance in the YADC group. These findings indicate distinct genus-level profiles across constitution groups.

Correlation between gut microbiota and clinical biochemical indicators

LEfSe analysis (with an LDA threshold set at 2) identified bacterial taxa that differed significantly across various constitution groups (Figures 4 A, B). The results revealed that *Parabacteroides* was significantly enriched in the BSC group, while the YADC group showed higher relative abundance of *Clostridium*. The YIDC group showed distinct bacterial features, with *Cellulosilyticum*, *Dorea*, and *Prevotella* being the most significant characteristic genera, with LDA scores greater than 3.

Further Spearman correlation analysis was performed to evaluate the relationships between gut microbiota and clinical biochemical indicators (Figure 4 C). At the phylum level, TG, TC, ALT, AST, and GLU were significantly positively correlated with the relative abundance of *Cyanobacteria* ($p < 0.05$). Additionally, at the order level, TG and TC were positively correlated with Cyanobacteria ($p < 0.05$), while GLU, ALT, and AST were positively correlated with *Acidobacteria* and *Thermoleophilia* ($p < 0.05$). GLU was negatively correlated with Bacilli ($p < 0.05$). At the genus level, AST positively correlated with UCG-002 ($p < 0.05$).

Fecal metabolomic features of MASLD patients

Figure 5 presents the total ion chromatograms of fecal samples from the PDC and DHC groups, with the strongest chromatographic peaks set at 100% relative abundance, reflecting the overall distribution characteristics of the fecal metabolites in both groups. The chromatograms show sharp peaks and good separation, with most metabolites detected between 5 and 19 min. Significant differences in peak intensities were observed between the groups: the PDC group exhibited higher peak intensities at 10.44 min and 17.35 min, while the DHC group showed higher peak intensities at 6.17 min and 18.51 min. Metabolite identification was conducted using MS-DIAL and the NIST database, leading to the identification of 106 metabolites, including small molecules such as amino acids and fatty acids.

Metabolite differential analysis among different TCM constitution groups

The PCA score plot (Figure 6 A) shows spatial separation between the metabolite profiles of the DHC and PDC groups, indicating differences in metabolic between the two groups. Further analysis using a volcano plot (Figure 6 B, Table II) with the thresholds of $p < 0.05$ and FC > 1.5 or < 0.667 revealed a total of 106 differential metabolites. Among the top 20 metabolites identified were lyxose, arabitol, iminodiacetic acid, quercetin, quinic acid, putrescine, sucrose, 1,2,4-benzenetriol, succinic acid, 4-hydroxy-3-methoxybenzoic acid, 4-nitrocatechol, glycerol-1-phosphate, inosine, O-phospho-serine, uracil, 4-pyridoxine, hydroquinone, caffeic acid, gallic acid, and 4-hydroxybenzoic acid. Notably, lyxose, arabitol, and iminodiacetic acid exhibited significant statistical differences ($p < 0.05$), suggesting their potential value in distinguishing the DHC and PDC groups. Heatmap analysis (Figure 6 C) further revealed clear clustering patterns in the metabolite expression profiles between the DHC and PDC group samples, showing distinct metabolic patterns between the two groups.

Functional annotation of differential metabolites and enrichment of metabolic pathways

Metabolic pathway enrichment analysis of differential metabolites between the DHC and PDC groups identified 15 significantly associated pathways (Figure 7, Table III). Among them, the biosynthesis of phenylalanine, tyrosine, and tryptophan (Pathway 1) and the metabolism of glycine, serine, and threonine (Pathway 2) showed the highest enrichment and topological impact, located in the

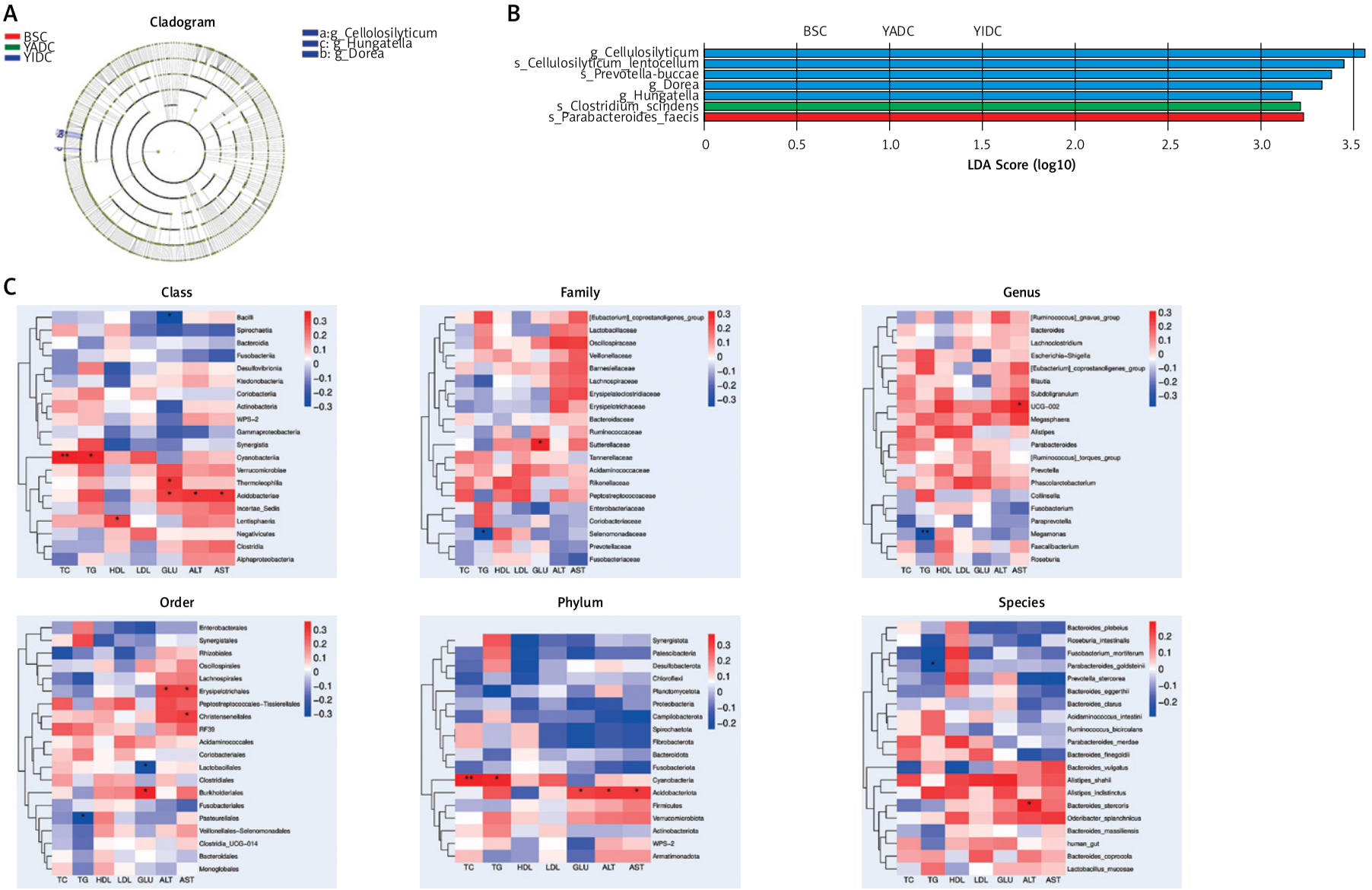

Figure 4. LEfSe analysis and correlation between gut microbiota and cytokines across different constitution groups. **A** – Overview dendrogram of LEfSe analysis; **B** – linear discriminant analysis (LDA) scores of specifically enriched genera in each group; **C** – Spearman correlation analysis of microbiota-cytokine relationships

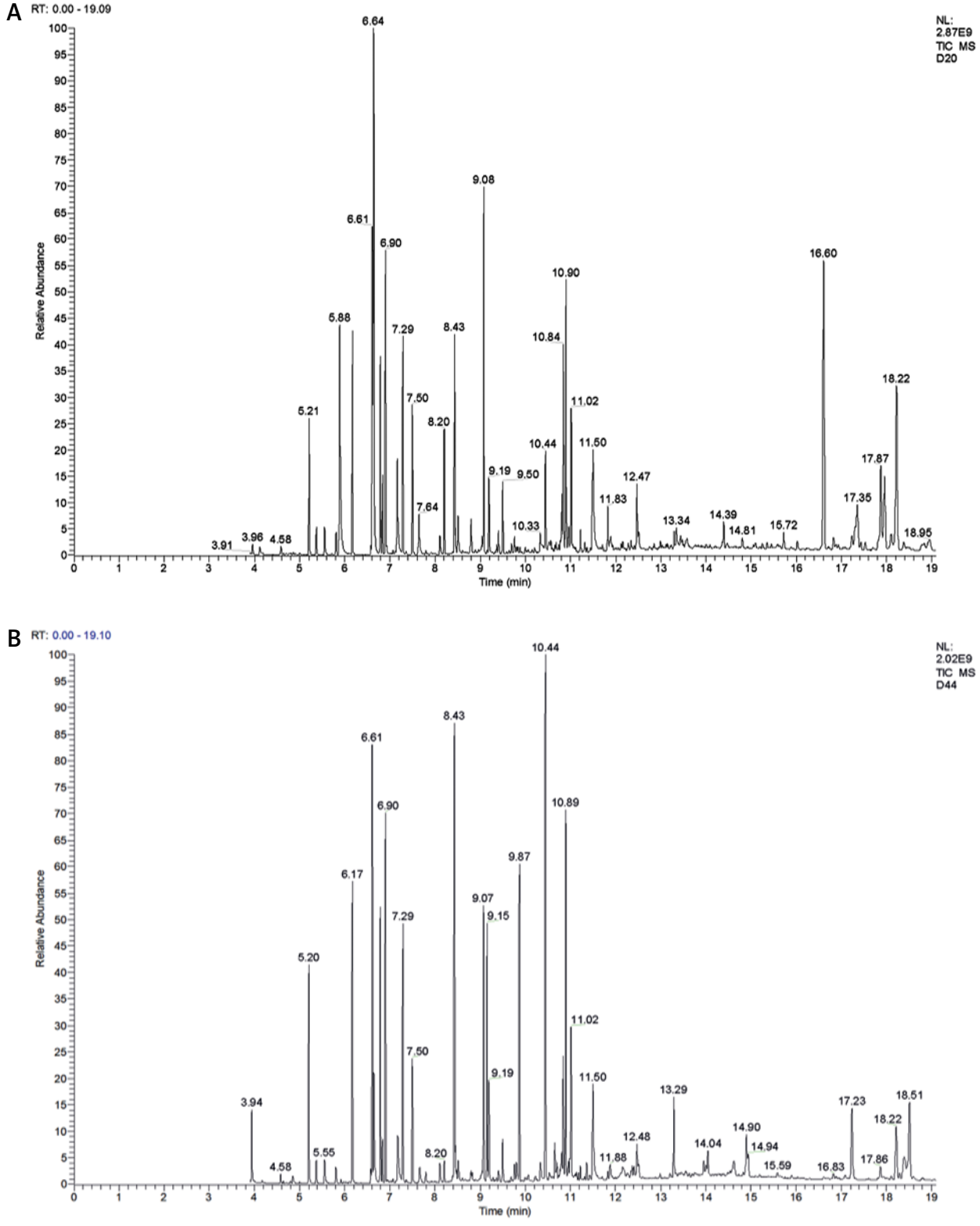

Figure 5. Gas chromatography-mass spectrometry total ion chromatogram analysis of fecal samples from phlegm-dampness and damp-heat constitution (DHC) groups. **A** – phlegm-dampness constitution (PDC) group; **B** – DHC group

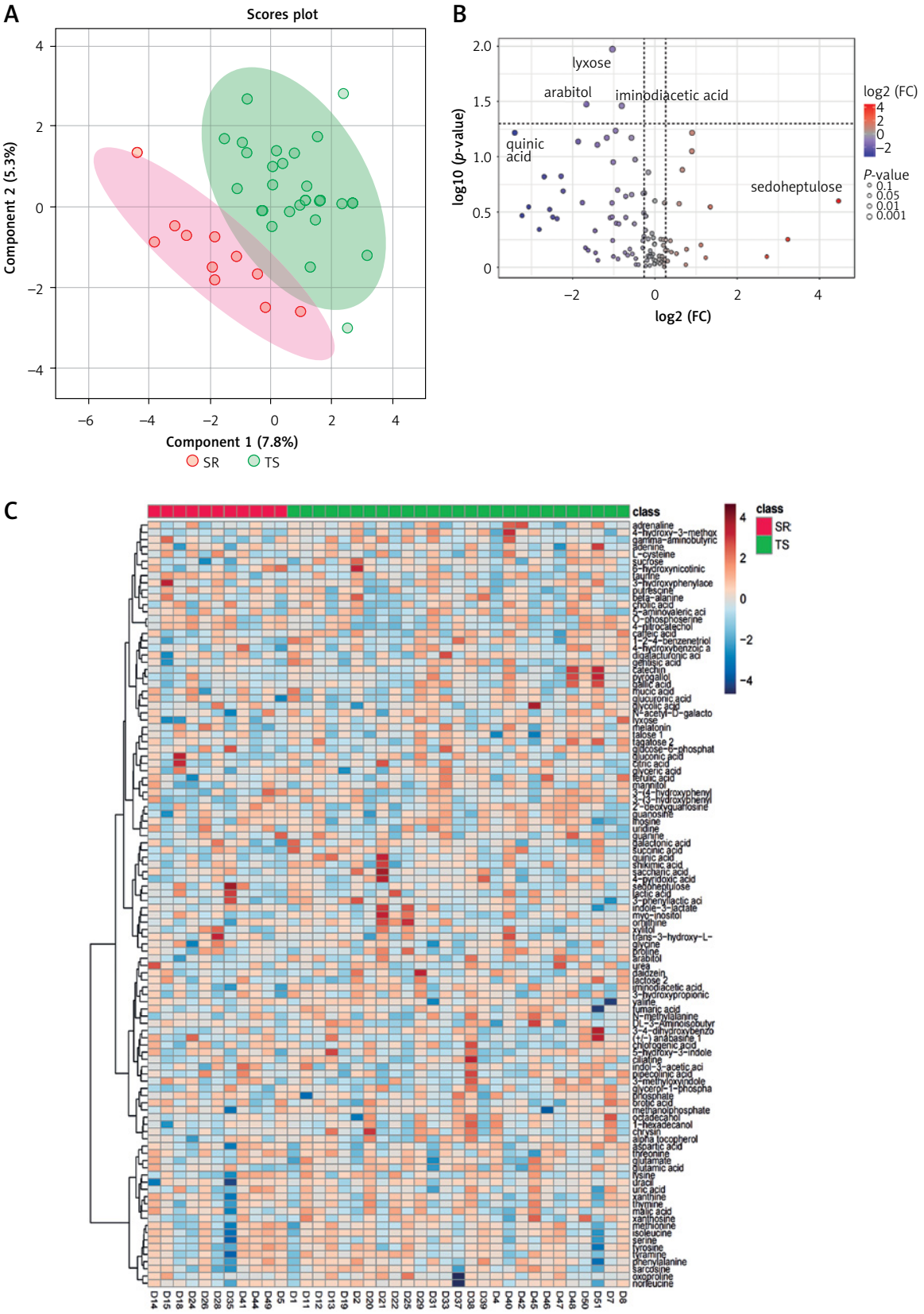

Figure 6. Differential fecal metabolites and distribution features between phlegm-dampness constitution (PDC) and damp-heat constitution (DHC) groups in metabolic dysfunction-associated steatotic liver disease (MASLD) patients. **A** – PCA of fecal samples from MASLD patients in both groups. SR = DHC group; TS = PDC group. **B** – Volcano plot showing differential ASVs between PDC and DHC groups. **C** – Heatmap illustrating the relative abundance of relevant taxonomic units in the PDC and DHC groups

Table II. Fecal metabolomic analysis of differential metabolites in DHC and PDC groups

No.	Metabolites	Fold change	*P*-value
		DHC/PDC	PDC/DHC
1	Lyxose	0.48965	0.010618
2	Arabitol	0.31528	0.033477
3	Iminodiacetic acid	0.57179	0.034533
4	Gentisic acid	0.51515	0.058056
5	Quinic acid	0.094409	0.06064
6	Putrescine	1.8711	0.060696
7	Sucrose	0.44471	0.067313
8	1,2,4-benzenetriol	0.67369	0.067334
9	Succinic acid	0.27505	0.072758
10	4-hydroxy-3-methoxybenzoic acid	0.37971	0.07803
11	4-nitrocatechol	1.8635	0.08902
12	Glycerol-1-phosphate	0.71656	0.10617
13	Xanthosine	0.49592	0.11173
14	O-phosphoserine	1.5873	0.13149
15	Uracil	0.89585	0.13815
16	4-pyridoxicacid	0.20601	0.14978
17	Pyrogallol	0.15497	0.15134
18	Caffeic acid	0.53365	0.20037
19	Gallic acid	0.21349	0.20443
20	4-hydroxybenzoicadd	0.83878	0.21276
21	3-(3-hydroxyphenyl)propionic acid	0.82316	0.21422
22	Mannitol	0.67599	0.22035
23	3-hydroxypropionicadd	0.61144	0.22793
24	3-phenyllactic acid	1.0008	0.25102
25	Sedoheptulose	22.023	0.25135
26	1-hexadecanol	0.29505	0.26001
27	Threonine	1.1805	0.26133
28	Myo-inositol	0.48606	0.26161
29	Taurine	1.5051	0.26594
30	Catechin	0.11953	0.28396
31	Rrans-3-hydroxy-L-proline	2.5432	0.28397
32	3-4-dihydroxybenzoic acid	0.16982	0.30015
33	Tyramine	0.82997	0.32175
34	Daidzein	0.10697	0.34115
35	N-acetyl-D-galactosamine	0.85874	0.34495
36	N-methylalanine	0.48751	0.35057

upper right quadrant of the pathway topology plot. Pathways 1 and 2 were both significantly enriched and exhibited high centrality within the metabolic network, indicating their potential involvement in the major metabolic distinctions between the DHC and PDC groups. Other pathways, including ascorbate metabolism and alanine, aspartate, and glutamate metabolism, also showed moderate enrichment, though with lower topological impact values. These results suggest that amino acid and energy metabolism pathways may be associated with the metabolic differences between the two constitution types.

Discussion

MASLD is a common metabolic liver disease characterized by hepatic steatosis (≥ 5% hepatic

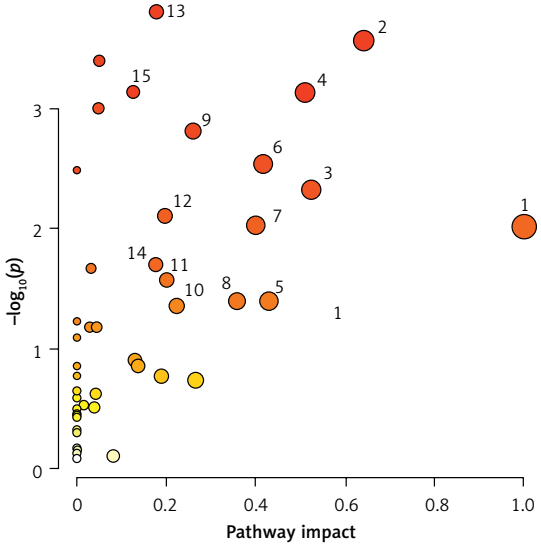

Figure 7. Bubble chart of metabolic pathway enrichment analysis for differential fecal metabolites between PDC and DHC groups. This figure presents the metabolic pathway enrichment analysis of differential metabolites performed using MetaboAnalyst 5.0. The size of the bubbles represents the topological impact value, and the color gradient from yellow to red indicates *p*-values from high to low (i.e., increasing significance). The numbers represent different metabolic pathways: (1) biosynthesis of phenylalanine, tyrosine, and tryptophan; (2) glycine, serine, and threonine metabolism; (3) ascorbate and aldarate metabolism; (4) alanine, aspartate, and glutamate metabolism; (5) taurine and hypotaurine metabolism; (6) arginine and proline metabolism; (7) β-alanine metabolism; (8) phenylalanine metabolism; (9) acetaldehyde and dicarboxylic acid metabolism; (10) cysteine and methionine metabolism; (11) tyrosine metabolism; (12) tricarboxylic acid cycle (TCA cycle); (13) arginine biosynthesis; (14) pyrimidine metabolism; (15) glutathione metabolism. The selection criteria were $p < 0.05$ and an impact value > 0.1. PDC: phlegm-dampness constitution, DHC: damp-heat constitution

fat) in the presence of cardiometabolic risk factors [14, 20]. It affects approximately 25–45% of the global population and is increasingly observed among younger individuals [21, 22]. This study, integrating microbiomics and metabolomics, identified TCM constitution-specific gut microbiota and metabolic signatures in MASLD (particularly in the DHC and PDC groups), highlighting alterations in microbiota diversity and metabolic pathways as potential mechanisms associated with disease characteristics and providing insights into personalized intervention strategies.

The results showed that MASLD patients exhibited reduced gut microbiota diversity and significant alterations in microbial composition, including increased relative abundances of *Firmicutes* and *Proteobacteria*, decreased *Bacteroidetes*, and a disrupted *Firmicutes*/*Bacteroidota* ratio [23]. At the constitution subtype level, microbiota profiles differed between DHC and PDC types. Notably, both groups showed elevated Proteobacteria, potentially linked to increased intestinal permeability and inflammation. From a TCM perspective, this may reflect a microbial distinction between "excess" and "deficiency" syndromes. Metabolomic analysis further revealed significant differences in glycine and aspartic acid levels between constitutions, suggesting potential associations with oxidative stress and energy metabolism regulation [24].

Further studies also confirmed constitution-specific gut microbiota signatures in NAFLD. The PDC group exhibited more pronounced dysbiosis, characterized by a lower *Firmicutes*/*Bacteroidetes* ratio, reduced *Faecalibacterium*, and elevated *Prevotella* abundance, which has been associated with inflammation and metabolic disruption [25]. Additionally, *Flavonifractor plautii* and its metabolite phytosphingosine were significantly reduced in PDC individuals, potentially leading to decreased PPARα pathway activity in the liver and contributing to altered lipid metabolism, even in individuals without overt metabolic abnormalities, indicating a potentially higher-risk metabolic profile [26]. In contrast, DHC patients showed elevated serum bile acids and downregulated protein expression, suggesting impaired systemic immune regulation and gut-liver axis dysfunction [27].

Both PDC and DHC types showed enrichment in amino acid metabolic pathways, particularly those involving phenylalanine, tyrosine, glycine, and serine, which have been implicated in oxidative stress, energy homeostasis, and inflammation [28]. The PDC group also showed increased metabolites such as lyxose and arabitol, suggesting alterations in carbohydrate metabolism [29]. Proteomic data further indicated that PDC patients showed evidence of increased JAK–STAT and PI3K–Akt signaling pathway activity, whereas DHC patients showed downregulation of immune-related proteins, suggesting constitution-specific differences in inflammatory and metabolic susceptibility [30]. Collectively, this study suggests an association among TCM constitution, gut microbiota, and metabolic alterations in MASLD, revealing distinct microbial, metabolic, and signaling features in DHC and PDC subtypes. These findings may provide a rationale for future personalized microbiota-targeted strategies based on constitution, such as modulating specific microbes or supplementing key metabolites, to improve the prevention and management of MASLD.

Despite these novel findings, several limitations exist. First, sample sizes for less common constitutions (e.g., qi stagnation, blood stasis, yang deficiency, yin deficiency) were small, and group

Table III. Results of pathway enrichment analysis of differential metabolites in serum samples

No.	Pathway	*P*-value	Impact	Metabolites
1	Phenylalanine, tyrosine and tryptophan biosynthesis	0.0095387	1	L-phenylalanine; L-tyrosine
2	Glycine, serine and threonine metabolism	0.00026861	0.64073	L-serine; glycine; O-phosphorylated L-serine; sarcosine; L-threonine; D-glycerate; L-cysteine
3	Ascorbate and aldarate metabolism	0.0047181	0.52381	Inositol; D-glucuronide; D-gluconate
4	Alanine, aspartate and glutamate metabolism	0.00072173	0.50962	L-aspartic acid; L-glutamic acid;4-aminobutyrate; citrate; fumarate; succinate
5	Taurine and hypotaurine metabolism	0.039993	0.42857	L-cysteine; taurine
6	Arginine and proline metabolism	0.0028753	0.41627	4-aminobutyrate; putrescine; trans-3-hydroxy-L-proline; L-proline,
7	Beta-alanine metabolism	0.0093132	0.39925	L-glutamic acid; L-ornithine; 3-hydroxypropionate; β-alanine; L-aspartic acid; uracil
8	Phenylalanine metabolism	0.039993	0.35714	L-phenylalanine; L-tyrosine
9	Glyoxylate and dicarboxylate metabolism	0.0015238	0.25927	Citrate; (S)-malic acid; L-serine; glycine; L-glutamic acid; D-glycerate
10	Cysteine and methionine metabolism	0.043963	0.22222	L-serine; L-methionine; L-cysteine; O-phosphorylated L-serine
11	Tyrosine metabolism	0.026728	0.20072	L-adrenaline; L-tyrosine; tyramine; fumarate; 2,5-dihydroxybenzoate
12	Citrate cycle (TCA cycle)	0.0077773	0.19704	Succinate; (S)-malate; citrate; fumarate
13	Arginine biosynthesis	0.00015406	0.17766	L-glutamic acid; L-aspartic acid; L-ornithine; urea; fumarate
14	Pyrimidine metabolism	0.019897	0.17576	Uridine; thymine; orotate; uracil; β-alanine
15	Glutathione metabolism	0.00072173	0.1261	Glycine; L-cysteine; L-glutamic acid; methylphenidate; L-ornithine; putrescine

merging may have obscured subtle differences. Second, 16S rRNA sequencing has limited taxonomic resolution and relies on predictive functional annotation, lacking direct functional evidence [31]. Third, participants were recruited from a single geographic region, and their gut microbiota may be influenced by local diet, lifestyle, and environment, which limits generalizability. Previous studies suggest that gut microbial changes may precede MASLD progression, emphasizing the need for time-series and multi-omics approaches [32], alongside standardized dietary assessments to reduce bias [33].

TCM constitution classification also remains partly subjective, despite existing criteria. Integrating genomics, epigenetics, and immunophenotyping could help identify objective biomarkers and enhance scientific rigor and global recognition of TCM constitution research [34]. Furthermore, liver function markers such as serum albumin should be included, as albumin not only reflects hepatic synthesis capacity but also exhibits esterase-like activity involved in lipid metabolism [35]; its reduction in NAFLD is associated with disease progression and dysbiosis [36]. Future research should incorporate metagenomics, transcriptomics, metabolomics, and single-cell technologies, along with germ-free animals, liver organoids, and *in vitro* models, to functionally validate constitution-related microbes and metabolites. Developing MASLD subtyping models based on TCM constitutions and confirming causality through animal and clinical studies will help bridge TCM theory with precision medicine and promote individualized interventions in MASLD.

In conclusion, this study revealed significant differences in the gut microbiota composition and metabolic characteristics of MASLD patients with different TCM constitutions, particularly between the DHC and PDC groups, showing constitution-specific changes in the microbiota (Graphic abstract). The associations between clinical indicators such as blood lipids and liver function and specific microbiota suggest that gut microbiota diversity and stability may be associated with the pathophysiology of MASLD. These findings may provide potential microbial targets for future constitution-related personalized diagnostic and therapeutic strategies for MASLD.

Funding

The research was financially supported by Changzhou Health and Health Youth Talent Training Project Funding (No. CZQM2022015).

Ethical approval

Approval number: 2023-LL-004(L).

Conflict of interest

The authors declare no conflict of interest.

References

1. Gerges SH, Wahdan SA, Elsherbiny DA, El-Demerdash E. Non-alcoholic fatty liver disease: an overview of risk factors, pathophysiological mechanisms, diagnostic procedures, and therapeutic interventions. Life Sci 2021; 271: 119220.
2. Dou L, Shi X, He X, Gao Y. Macrophage phenotype and function in liver disorder. Front Immunol 2020; 10: 3112.
3. Draijer L, Benninga M, Koot B. Pediatric NAFLD: an overview and recent developments in diagnostics and treatment. Expert Rev Gastroenterol Hepatol 2019; 13: 447-61.
4. Powell EE, Wong VWS, Rinella M. Non-alcoholic fatty liver disease. Lancet 2021; 397: 2212-24.
5. Govaere O, Petersen SK, Martinez-Lopez N, et al. Macrophage scavenger receptor 1 mediates lipid-induced inflammation in non-alcoholic fatty liver disease. J Hepatol 2022; 76: 1001-12.
6. Jiang W, Wu N, Wang X, et al. Dysbiosis gut microbiota associated with inflammation and impaired mucosal immune function in intestine of humans with non-alcoholic fatty liver disease. Sci Rep 2015; 5: 8096.
7. Aron-Wisnewsky J, Vigliotti C, Witjes J, et al. Gut microbiota and human NAFLD: disentangling microbial signatures from metabolic disorders. Nat Rev Gastroenterol Hepatol 2020; 17: 279-97.
8. Oh TG, Kim SM, Caussy C, et al. A universal gut-microbiome-derived signature predicts cirrhosis. Cell Metabolism 2020; 32: 878-88.
9. Gill K, Bindal E, Garg P, Kumar D, Bhattacharyya R, Banerjee D. Exposure of bisphenols (BPA, BPB and BPC) in HepG2 cells results in lysosomal dysfunction and lipid accumulation. Cell Biology Int 2025; 49: 709-22.
10. Li CL, Yao ZY, Zhang YF, et al. Bisphenols exposure and non-alcoholic fatty liver disease: from environmental trigger to molecular pathogenesis. Front Endocrinol 2025; 16. doi:10.3389/fendo.2025.1606654
11. Feng D, Zhang H, Jiang X, et al. Bisphenol A exposure induces gut microbiota dysbiosis and consequent activation of gut-liver axis leading to hepatic steatosis in CD-1 mice. Environ Pollut 2020; 265: 114880.
12. Jasirwan COM, Muradi A, Hasan I, Simadibrata M, Rinaldi I. Correlation of gut Firmicutes/Bacteroidetes ratio with fibrosis and steatosis stratified by body mass index in patients with non-alcoholic fatty liver disease. Biosci Microbiota Food Health 2021; 40: 50-8.
13. Yu JS, Youn GS, Choi J, et al. Lactobacillus lactis and Pediococcus pentosaceus-driven reprogramming of gut microbiome and metabolome ameliorates the progression of non-alcoholic fatty liver disease. Clin Transl Med 2021; 11: e634.
14. Zhu M, Dagah OMA, Silaa BB, Lu J. Thioredoxin/glutaredoxin systems and gut microbiota in NAFLD: interplay, mechanism, and therapeutical potential. Antioxidants 2023; 12: 1680.
15. Nowiński A, Ufnal M. Gut bacteria-derived molecules as mediators and markers in cardiovascular diseases. The role of the gut-blood barrier. Kardiol Pol 2018; 76: 320-7.
16. Loomba R, Seguritan V, Li W, et al. Gut microbiome-based metagenomic signature for non-invasive detection of advanced fibrosis in human nonalcoholic fatty liver disease. Cell Metabol 2019; 30: 607.
17. Yamashiro K, Kurita N, Urabe T, Hattori N. Role of the gut microbiota in stroke pathogenesis and potential therapeutic implications. Ann Nutr Metab 2021; 77 (Suppl. 2): 36-44.
18. Li Y, Ji X, Wu H, Li X, Zhang H, Tang D. Mechanisms of traditional Chinese medicine in modulating gut microbiota metabolites-mediated lipid metabolism. J Ethnopharmacol 2021; 278: 114207.
19. Zhang R, Gao X, Bai H, Ning K. Traditional Chinese medicine and gut microbiome: their respective and concert effects on healthcare. Front Pharmacol 2020; 11: 538.
20. Fan JG, Kim SU, Wong VWS. New trends on obesity and NAFLD in Asia. J Hepatol 2017; 67: 862-73.
21. Wang T, Guo XK, Xu H. Disentangling the progression of non-alcoholic fatty liver disease in the human gut microbiota. Front Microbiol 2021; 12: 728823.
22. Chen J, Vitetta L. Gut microbiota metabolites in NAFLD pathogenesis and therapeutic implications. IJMS 2020; 21: 5214.
23. Fang J, Yu CH, Li XJ, et al. Gut dysbiosis in nonalcoholic fatty liver disease: pathogenesis, diagnosis, and therapeutic implications. Front Cell Infect Microbiol 2022; 12: 997018.
24. Rom O, Liu Y, Liu Z, et al. Glycine-based treatment ameliorates NAFLD by modulating fatty acid oxidation, glutathione synthesis, and the gut microbiome. Sci Transl Med 2020; 12: eaaz2841.
25. Shin J, Li T, Zhu L, et al. Obese individuals with and without phlegm-dampness constitution show different gut microbial composition associated with risk of metabolic disorders. Front Cell Infect Microbiol 2022; 12: 859708.
26. Li L, Li T, Liang X, et al. A decrease in Flavonifractor plautii and its product, phytosphingosine, predisposes individuals with phlegm-dampness constitution to metabolic disorders. Cell Discov 2025; 11: 25.
27. Pan Y, Guo J, Hu N, et al. Distinct common signatures of gut microbiota associated with damp-heat syndrome in patients with different chronic liver diseases. Front Pharmacol 2022; 13: 1027628.
28. Zhang F, Wu J, Ruan H, et al. ZeXie decoction alleviates non-alcoholic fatty liver disease in rats: the study of genes, lipids, and gut microbiotas. Biochem Biophys Res Commun 2022; 632: 129-38.
29. Zhao H, Zong Y, Li W, et al. Damp-heat constitution influences gut microbiota and urine metabolism of Chinese infants. Heliyon 2023; 9: e12424.
30. Chen X, Tan F, Zhang H, et al. Serum cytokine profiles in phlegm-dampness constitution and damp-heat constitution using proteomic antibody microarray. Eur J Integr Med 2022; 52: 102126.
31. Nakagawa H, Saio T, Nagao M, et al. Conformational dynamics of a multidomain protein by neutron scattering and computational analysis. Biophys J 2021; 120: 3341-54.
32. Rabe M, Toparli C, Chen YH, Kasian O, Mayrhofer KJJ, Erbe A. Alkaline manganese electrochemistry studied byin situandoperandospectroscopic methods – metal

dissolution, oxide formation and oxygen evolution. Phys Chem Chem Phys 2019; 21: 10457-69.
33. Smalley CM, Fertel BS, McShane AJ, Cremer PC, Muir MR, Mentias A. Outcomes in emergency department patients with intermediate elevations in high-sensitive cardiac troponin T. Am J Emerg Med 2023; 65: 212-3.
34. Shen S, Zhong H, Zhou X, et al. Advances in traditional chinese medicine research in diabetic kidney disease treatment. Pharm Biol 2024; 62: 222-32.
35. Kumar D, Behal S, Bhattacharyya R, Banerjee D. Pseudoesterase activity of albumin: a probable determinant of cholesterol biosynthesis. Med Hypoth 2018; 115: 42-5.
36. Wang S, Lin X, Zhu C, et al. Association between nonalcoholic fatty liver disease and increased glucose-to-albumin ratio in adults without diabetes. Front Endocrinol 2024; 14: 1287916.